**Supplementary Information**

# Conjugation of Bone Graft with NO-delivery Dinitrosyl Iron Complexes Promotes Synergistic Osteogenesis and Angiogenesis in Rat Calvaria Bone Defects

Shih-Hao Chang,[1,2,3] Hui-Yi Hsiao,[*3,4,5] Yi-Hong Chen,[6] Ming-Huei Cheng,[3,4] Jia-Wei Liu,[3,4] Hsiao-Jo Huang,[1,3] Yu-Ting Chou,[7] Tarik Abdelkareem Mostafa Amer,[7] Priya Vijayaraghavan,[8] Sathyadevi Palanisamy,[6] Yun-Ming Wang,[*7,9] Tsai-Te Lu[*6,10,11]

**Affiliations:**

[1]Department of Periodontics, Linkou Chang Gung Memorial Hospital, Taoyuan 33305, Taiwan.
[2]Graduate Institute of Dental and Craniofacial Science, Chang Gung University, Taoyuan 33302, Taiwan.
[3]Center of Tissue Engineering, Linkuo Chang Gung Memorial Hospital, Taoyuan 33305, Taiwan.
[4]Division of Reconstructive Microsurgery, Department of Plastic and Reconstructive Surgery, Linkou Chang Gung Memorial Hospital, Taoyuan 33305, Taiwan.
[5]Department of Biomedical Sciences, Chang Gung University, Taoyuan 33302, Taiwan.
[6]Institute of Biomedical Engineering, National Tsing Hua University, Hsinchu 30013, Taiwan.
[7]Department of Biological Science and Technology, Institute of Molecular Medicine and Bioengineering, College of Biological Science and Technology, National Yang Ming Chiao Tung University, Hsinchu 300, Taiwan.
[8]Graduate Institute of Medicine, Kaohsiung Medical University, Kaohsiung 807, Taiwan.
[9]Center for Intelligent Drug Systems and Smart Bio-devices (IDS2B), National Yang Ming Chiao Tung University, Hsinchu 300, Taiwan.
[10]Department of Chemistry, National Tsing Hua University, Hsinchu 30013, Taiwan.
[11]Department of Chemistry, Chung Yuan Christian University, Taoyuan 32023, Taiwan.

[*]**Corresponding author:**
Hui-Yi Hsiao, Ph.D. E-mail: ivyhsiao@gmail.com; Yun-Ming Wang, Ph.D. E-mail: ymwang@mail.nctu.edu.tw; Tsai-Te Lu, Ph.D. E-mail: ttlu@mx.nthu.edu.tw.

**Keywords:** Nitric Oxide, Dinitrosyl Iron Complexes, Angiogenesis, Osteogenesis

## Material and Methods

**Reagents.** The reagents sodium chloride (NaCl) from Merck; potassium chloride (KCl), disodium hydrogen phosphate ($Na_2HPO_4$), and potassium dihydrogen phosphate ($KH_2PO_4$) from Showa, deproteinized bovine bone mineral (DBBM, Bio-Oss™, 250-1000 μm) from Geistlich Pharma; and β-tricalcium phosphate (TCP, Cerasorb™, 500~1000 μm) from Curasan of analytical grade were used as received. Double-distilled water was obtained using a Millipore water distilling apparatus (USA). Complexes $[Fe_2(\mu\text{-}SCH_2CH_2COOH)_2(NO)_4]$ (**DNIC-COOH**), $[(NO)_2Fe(\mu\text{-}S\text{-}thioglycerol)_2Fe(NO)_2]$ (**DNIC-TG**), and $[Fe_2(\mu\text{-}SCH_2CH_2OH)_2(NO)_4]$ were synthesized based on published procedures.[1, 2]

**Instruments.** All the EPR measurements were performed at X-band using a Bruker EMXmicro-6/1/S/L spectrometer equipped with a Bruker E4119001 super high sensitivity cavity. X-band EPR spectra were obtained with a microwave power of 0.6456- 0.6348 mW, frequency at 9.41 GHz, conversion time of 66.68 ms, receiver gain of 30, and modulation amplitude of 10.0 G at 100 KHz. UV-vis spectra were recorded on a Perkin-Elmer Lambda 365 spectrometer. Solid-state Fourier-transform infrared (FT-IR) spectra were recorded on a Perkin-Elmer spectrum two spectrophotometers with pressed KBr pellets, whereas the FT-IR spectrum of **DNIC-COOH** in THF was recorded using a sealed solution cell (0.1 mm, $CaF_2$ windows). Powder X-ray diffraction (PXRD) patterns were recorded with an X-ray diffractometer (Bruker D2 Phaser) using Cu $K_\alpha$ radiation ($\lambda$= 1.5418 Å). Morphology of DBBM and DNIC-DBBM were imaged by field-emission scanning electron microscope (FESEM, JEOL JSM-7000F). The elemental mapping images and energy-dispersive X-ray spectroscopy (EDS) analysis of DBBM and DNIC-DBBM were acquired on a SEM-

EDS attachment equipped on FESEM (JEOL JSM-7000F). The confocal microscopic images were recorded using Leica TCS-SP-X AOBS or ZEISS LSM 780 confocal microscope systems.

**Preparation of $[(NO)_2Fe(\mu\text{-}SCH_2CH_2COOMe)_2Fe(NO)_2]$ (DNIC-COOMe).** A THF solution of $[Fe(CO)_2(NO)_2]$ was freshly prepared by reaction of [Na-18-crown-6-ether][$Fe(CO)_3(NO)$] (1.450 g, 3.17 mmol) and [NO][$BF_4$] (0.365 g, 3.15 mmol) ) in a 50-mL Schlenk flask. Compound 3-methyl-mercaptopropionate (179 μL, 2 mmol) was then added into this THF solution of $[Fe(CO)_2(NO)_2]$ via a gas-tight syringe. After the reaction solution was stirred at ambient temperature for 3 days, distinctive IR $\nu_{NO}$ stretching frequencies at 1778 and 1758 $cm^{-1}$ indicate the formation of $[(NO)_2Fe(\mu\text{-}SCH_2CH_2COOMe)_2Fe(NO)_2]$ (**DNIC-COOMe**). Solvent was removed under vacuum before the crude brown solid was dissolved in 15 mL of n-hexane. After filtration through Celite, solvent was then removed under vacuum to yield dark-brown solid **DNIC-COOMe** (yield 0.19 g, 40.9%). IR $\nu_{NO}$ (THF): 1778 (s), 1758 (s) $cm^{-1}$.

**Preparation of $[(NO)_2Fe(\mu\text{-}SCH_2CH_2COONa)_2Fe(NO)_2]$ (DNIC-COONa). DNIC-COOH** (0.044 g, 0.1 mmol) was dissolved in 1 mL of 0.2 M $NaOH_{(aq)}$ solution under $N_{2(g)}$. This reaction solution was stirred at ambient temperature under $N_{2(g)}$ for 10 min before this solution was lyophilized to yield dark-brown soild **DNIC-COONa**. IR $\nu_{NO}$ (KBr): 1768 s and 1758 $cm^{-1}$.

**NO-release Reactivity of Different DNICs in αMEM without/with the presence of 10% FBS or BSA.** 50 μM of **DNIC-COOH** was prepared via addition of 20 μL of a 50-mM stock solution of **DNIC-COOH** in DMSO to 19.98 mL of αMEM (Gibco™). After this solution was incubated at 37 °C under aerobic condition for 0, 0.5, 1, 2, 3, 4,

6, 8, and 24 h, 40-μL aliquots of this solution was collected to evaluate the release of NO using Nitrate/Nitrite Colorimetric Assay Kit (Item No. 780001, Cayman). A general procedure is described as below. After 40 μL of the aqueous solution derived from degradation of **DNIC-COOH** was diluted with 40 μL of kit assay buffer, 10 μL of Enzyme Cofactor Mixture (Item No. 780012) and 10 μL of Nitrate Reductase Mixture (Item No. 780010) were added before this mixture solution was covered and incubated at room temperature for 1 h. Subsequent addition of 50 μL of Griess Reagent R1 (Item No. 780018) and 50 μL of Griess Reagent R2 (Item No. 780020) followed by incubation at room temperature for 15 min results in the formation of UV-vis absorption band at 540 nm. The absorbance at 540 nm was then recorded using a microplate reader (SpectraMax iD3, Molecular Devices, San Jose, CA, USA) with a reference wavelength of 800 nm. According to a calibration curve made with 0, 5, 10, 15, 20, 25, 30, and 35 μM of nitrite standard (Item No. 780016)/nitrate standard (Item No. 780014), respectively, NO-release reactivity of **DNIC-COOH** in αMEM was further estimated. Assuming that the aerobic degradation of **DNIC-COOH** follows pseudo-first order kinetics, half-life for the release of NO from **DNIC-COOH** in αMEM at 37 $^{o}$C was further determined. Three independent experiments were executed to measure the average half-life for release of NO from **DNIC-COOH** in αMEM at 37 $^{o}$C.

Average half-life for release of NO from (1) **DNIC-COOH** in αMEM with the presence of 10% fetal bovine serum (FBS, Gibco™), (2) **DNIC-COOH** in αMEM with the presence of bovine serum albumin (BSA, 50 mg/mL, Sigma-Aldrich), (3) **DNIC-TG** in αMEM, (4) **DNIC-TG** in αMEM with the presence of 10% FBS, (5) **DNIC-TG** in αMEM with the presence of BSA (50 mg/mL), (6) **DNIC-COOMe** in αMEM, (7) **DNIC-COOMe** in αMEM with the presence of 10% FBS, and (8) **DNIC-COOMe** in

αMEM with the presence of BSA (50 mg/mL) at 37°C was determined in a similar manner.

**EPR Investigations on Assembly of Protein-bound DNIC derived from DNICs in αMEM with the presence of 10% FBS or BSA.** 100 μM of **DNIC-COOH** was prepared via addition of 20 μL of a 100-mM stock solution of **DNIC-COOH** in DMSO to 19.98 mL of αMEM with the presence of 10% FBS. After this solution was incubated at 37°C for 0, 0.5, 1, 2, 3, 4, 8, and 24 h, respectively, EPR spectra for 100-μL aliquots of this solution was measured to characterize the time-dependent formation and degradation of the albumin BSA-bound DNIC. EPR investigations on the formation and degradation of the albumin BSA-bound DNICs upon (1) incubation of 100 μM of **DNIC-COOH** in αMEM with the presence of BSA (50 mg/mL), (2) incubation of 10 μM of **DNIC-TG** in αMEM with the presence of 10% FBS, (3) incubation of 10 μM of **DNIC-TG** in αMEM with the presence of BSA (50 mg/mL), (4) incubation of 10 μM of **DNIC-COOMe** in αMEM with the presence of 10% FBS, (5) incubation of 10 μM of **DNIC-COOMe** in αMEM with the presence of BSA (50 mg/mL) were performed in a similar manner. In addition, EPR spectra for 100 μM of **DNIC-COOH** in αMEM, 10 μM of **DNIC-TG** in αMEM, and 10 μM of **DNIC-COOMe** in αMEM were also measured.

**Cells.** A mouse calvaria preosteoblast cell line, MC3T3-E1, was purchased from ATCC (lot: CRL-2594), whereas a human umbilical vein endothelial (HUVEC) cell line was purchased from Blossom Biotechnologies, Inc (New Taipei City, Taiwan). The MC3T3-E1 cells were cultured in Minimum Essential Medium Eagle Alpha Modification (αMEM) without ascorbic acid (#A1049001, Gibco™) supplemented with 10% fetal bovine serum (Gibco™ or Hyclone™) and 1% penicillin/streptomycin

(Invitrogen); the HUVEC cells were cultured in Medium 199 (#31100035, Gibco™) supplemented with 10% heat-inactivated fetal bovine serum (#SH30396.03, Hyclone™), heparin (25 U/mL, #H3149, Sigma-Aldrich), endothelial cell growth supplement (30 μg/mL, ECGS; #02-102, Sigma-Aldrich), and 1% penicillin/streptomycin (#SV30010, Hyclone™). The MC3T3-E1 cells and HUVEC were incubated in T75 flask at 37°C in 5% $CO_2$ humidified air and the culture medium was refreshed every other day.

**Cell Viability Study of MC3T3-E1 Osteoblast Cells and HUVEC.** Cell viability study of osteoblast MC3T3-E1 cells with or without the treatment of **DNIC-COOH** was measured using a Cell Counting Kit-8 (Dojindo, FoliBio) according to the manufacturer's protocol. Briefly, osteoblast MC3T3-E1 cells were seeded into a 96-well plate at a density of $2.5\times10^3$ cells/well and incubated overnight. Next day, osteoblast MC3T3-E1 cells were treated with **DNIC-COOH** at different concentrations (0, 10 nM, 100 nM, 1 μM, 10 μM, 100 μM, and 1 mM) and incubated for 24 h. Culture media were then removed before the osteoblast MC3T3-E1 cells were washed with DPBS. After addition of fresh medium containing CCK-8 solution to the osteoblast MC3T3-E1 cells and incubated for 1 h, the absorbance at 450 nm was then measured on a microplate reader (SpectraMax iD3, Molecular Devices, San Jose, CA, USA) with a reference wavelength of 650 nm. Three independent experiments were executed and the result was represented as mean±SD% (n = 3) with the untreated cells (control) as 100% viability. Cell viability study of osteoblast MC3T3-E1 cells (1) with the treatment of **DNIC-TG**/**DNIC-COOMe** for 24 h, (2) with the sequential treatments of ODQ (1 h) and **DNIC-COOH** for 24 h, and (3) with the co-treatments of PTIO and **DNIC-COOH** for 24 h, respectively, was performed in a similar manner.

Cell viability study of HUVEC with or without the treatment of **DNIC-COOH** for 24 h and 48 h, respectively, was perform using MTT assay and represented as mean±SD% (n = 3) with the untreated cells (control) as 100% viability.

**VEGF-A and CD31 Measurements in HUVEC.** The HUVEC cells were seeded on a cover glass (12 mm in diameter) loaded in a 24-well plate at a density of $2.5 \times 10^4$ cells/well until the desired confluency is reached. After the culture media were removed, **DNIC-COOH** (3.9 μM or 7.8 μM) were then added to the cell culture and incubated for 24 h. Then the culture media were removed, and the cells were washed three times with PBS before the cells were fixed with 4% paraformaldehyde (PFA) solution for 10 min at room temperature. After the PFA solution is removed and the cells were washed with PBS, the cells were permeabilized with 0.1%-0.25% Triton X-100/PBS (or 0.5% saponin/PBS) at room temperature for 15 min. Subsequently, the HUVEC cells were washed with PBS for three times and incubated with a blocking buffer (3% BSA in PBS) at room temperature for 1 h. Then, the HUVEC cells were incubated with primary antibody solution (1:500 for Alexa Fluor® 594 anti-human CD31 antibody, cat. No. 303126, Biolegend company, Taiwan; 1:500 for VEGF-A antibody GeneTex company, Taiwan) at 4°C overnight before the HUVEC cells were washed with PBS for three times. The HUVEC cells were further incubated with a secondary antibody (1:500, Goat anti-mouse IgG DyLight™ 488 antibody, cat. No. GTX21316, GeneTex company, Taiwan) in the blocking buffer at room temperature for 1 h, and then washed with PBS. Cover glasses containing fixed cells were mounted onto a microscope slide loaded with Fluoroshield™ mounting medium with DAPI to stain the nuclei before the optical images were captured using a confocal imaging system (Leica TCS-SP-X AOBS).

**Scratch Assay for Cell Migration.** To investigate the migratory ability of HUVEC cells without (control group) or with the treatment of different concentrations of **DNIC-COOH**, the scratch wound healing assay was conducted. Briefly, the HUVEC cells were seeded in a 6-well culture plate at a density of $1 \times 10^4$ per well and allowed to get a confluent HUVEC monolayer through culturing in an incubator at 37 °C for 24 h. Afterwards, a straight-lined wide scratch of 1 mm width was made on the cell monolayer using a pipette tip to obtain an incisional wound before the sample treatments into the culture dishes containing fresh culture medium supplemented with 5% FBS. Then, cells were washed with PBS to remove the debris and further treated with **DNIC-COOH** (3.9 μM or 7.8 μM), which is followed by incubation for additional 24 h. The cells were photographed at desired time intervals to analyze the rate of cell migration, and the percentage of cell migration was calculated according to the following equation:

$$\text{Cell migration } (\%) = \left[\frac{A_0 - A_t}{A_0} \times 100\right]$$

'$A_0$' is the scratch area without treatment at 0 h and '$A_t$' is the scratch area after treatment at various time intervals.

**Tube Formation Assay.** To investigate the pro-angiogenesis activity of the **DNIC-COOH**, a tubule formation assay was performed. A 24-well culture plate was coated with growth factor-reduced Matrigel (60 μL/well) and pre-incubated for 30 min at 37 °C. Before the treatment of **DNIC-COOH** (3.8 μM or 7.8 μM), HUVEC cells were cultured in the above-mentioned 24-well plates at a density of $2 \times 10^4$ cells/well and incubated for 24 h. The formation of tubule junctions, tubule meshes, and tubule nodes was digitally imaged and analyzed using the ImageJ software.

**EPR Investigations on Cellular Uptake of DNICs and Intracellular Formation/Decomposition of Protein-bound DNICs in MC3T3-E1 Osteoblast Cells.** Cellular uptake of **DNIC-COOH** and intracellular formation/decomposition of protein-bound DNICs in osteoblast MC3T3-E1 cells were investigated using EPR. Briefly, osteoblast MC3T3-E1 cells were seeded into two 100-mm dishes at a density of $2\times10^6$ cells and incubated at 37°C overnight. Next day, osteoblast MC3T3-E1 cells were treated with 100 μM of **DNIC-COOH** and incubated for 0, 0.5, 1, 2, 3, 4, 8, and 24 h, respectively. After removal of the supernatant solution, osteoblast MC3T3-E1 cells were further washed with DPBS before addition of 1 mL of trypsin/EDTA (0.05%/0.53 mM) and incubation for 5 min at 37°C. After the obtained cell suspension solutions from two 100-mm dishes was combined and further centrifuged at 800 g for 5 min, the supernatant was removed before addition of 100 μL of αMEM. This solution was then transferred into EPR quartz tube and frozen in $N_{2(l)}$ before the EPR measurements.

Time-dependent decay of EPR signal intensity after treatment of **DNIC-COOH** for 2 h was then fit to pseudo-first order kinetics in order to determine the intracellular half-life for protein-bound DNIC. Three independent experiments were executed to measure the average half-life for intracellular decomposition of protein-bound DNICs in osteoblast MC3T3-E1 cells after treatment of 100 μM of **DNIC-COOH** at 37 $^{o}$C.

Cellular uptake of **DNIC-COOH** (10 μM)/**DNIC-TG** (10 μM)/**DNIC-COOMe** (10 μM) and intracellular formation/decomposition of protein-bound DNICs in osteoblast MC3T3-E1 cells were investigated using EPR in a similar manner.

**Kinetic Study on Intracellular Release of NO in MC3T3-E1 Osteoblast Cells after Treatment of DNICs.** Intracellular delivery of NO by **DNIC-COOH** was validated

using the fluorescence probe 4-amino-5-methylamino-2',7'-difluorofluorescein diacetate (DAF-FM) in combination fluorescence techniques. Osteoblast MC3T3-E1 cells were seeded into a 96-well black plate at a density of $5\times10^3$ cells and incubated at 37°C overnight. Next day, osteoblast MC3T3-E1 cells were first treated with 5 μM of DAF-FM and incubated at 37°C for 0.5 h. After removal of the supernatant solution, 100 μM of **DNIC-COOH** was added and incubated for 0, 1, 2, 4, 6, and 8 h, respectively, in the dark. Fluorescence intensity of the cells was then recorded using a microplate reader (SpectraMax iD3, Molecular Devices, San Jose, CA, USA) with an excitation wavelength at 485 nm and an emission wavelength at 525 nm. Three independent experiments were executed to measure the time-dependent change of average fluorescence intensity. Time-dependent change of average fluorescence intensity for the osteoblast MC3T3-E1 cells (1) with the treatment of 5 μM of DAF-FM, (2) with sequential treatment of 5 μM of DAF-FM and 10 μM of **DNIC-COOH**, or (3) with sequential treatment of 5 μM of DAF-FM and 10 μM of **DNIC-TG**, or (4) with sequential treatment of 5 μM of DAF-FM and 10 μM of **DNIC-COOMe** was determined in a similar manner.

Confocal microscopy images for the osteoblast MC3T3-E1 cells with sequential treatment of 5 μM of DAF-FM and 500 μM of **DNIC-COOH** was taken following the procedure described below. The osteoblast MC3T3-E1 cells were plated in 12-well plates at a density of $2.5 \times 10^4$ cells/well on cover glasses (18 mm in diameter) for 24 h and incubated with 5 μM DAF-FM for 0.5 h. After the culture media were removed, **DNIC-COOH** (500 μM) were then added to the cell culture and incubated for 1 h. Then the culture media were removed, and the cells were washed three times with PBS before the cells were fixed with 4% formaldehyde solution for 15 min at room temperature.

Cell nuclei were stained with 4′-6-diamidino-2-phenylindole (DAPI, blue). Cover glasses containing fixed cells were mounted in mounting medium (FluoroQuest™) on a microscope slide, and the optical images were captured using a confocal imaging system (ZEISS, LSM 780). Confocal microscopy images for the osteoblast MC3T3-E1 cells with the treatment of (1) 5 μM of DAF-FM, (2) with sequential treatment of 5 μM of DAF-FM and 50 μM of **DNIC-TG**, and (3) with sequential treatment of 5 μM of DAF-FM and 50 μM of **DNIC-COOMe**, respectively, were also taken in a similar manner.

**Western Blot Analysis.** MC3T3-E1 osteoblast cells were seeded into a 6-well plate at a density of $1\times10^6$ cells/well and incubated at 37°C overnight. Next day, osteoblast MC3T3-E1 cells were treated with 100 μM of **DNIC-COOH** and incubated for 24 h. Afterwards, the DNIC-treated cells were washed with ice-cold PBS and lysed by RIPA lysis buffer with protease inhibitor (#786-108, G-Biosciences). Lysates were sonicated to complete the lysis and DNA shearing. Protein concentrations were quantified by the PierceTM BCA protein assay kit (#23227, Thermo Scientific). Equal amounts of proteins were separated on SDS-PAGE and then electrophoretically transferred to PVDF membranes. Non-specific bindings were blocked by 5% skim milk or BSA in TBS-T. Blots were then probed with primary antibodies against PKG2 (1:1000) (#55138-1-AP, proteintech), ENaC-α (1:1000) (#SPC-403, stressmarq), HIF-1α (1:1000) (#tcea9197, Taiclone), VEGF (1:1000) (#tcba2323, Taiclone), β-catenin (1:1000) (#Tcea21793, Taiclone), SHP-1 (1:1000) (#3759, Cell signaling), SHP-2 (1:1000) (#3397, Cell signaling), p-Src (1:1000) (#2101, Cell signaling), Src (1:1000) (#2109, Cell signaling), and p-Akt (1:1000) (#66444-1-Ig, proteintech), respectively, at 4°C for overnight. After being washed three times with TBS-T, the membrane was

incubated with horseradish peroxidase-conjugated secondary antibody (#7074S or #7076S, Cell signaling) for 1 h at room temperature. Enhanced chemiluminescence (ECL; #34580, Thermo Scientific) was used and signals were detected by luminescence image system (Hansor, Taiwan).

**Preparation of DNIC-DBBM.** To a 15-mL centrifuge tube loaded with DBBM (0.100 g) and **DNIC-COOH** (0.010 g, 0.023 mmol), 2 mL of THF was added via stainless cannula under positive $N_{2(g)}$ pressure. After this reaction solution was shaken at ambient temperature for 1 h, the supernatant solution was removed before the residual solid was washed with THF three times and dried under vacuum. The distinctive IR $\nu$NO stretching frequencies at (1814, 1772, 1746) $cm^{-1}$ and PXRD peaks at $2\theta$ = 25.47°, 31.64°, 32.59°, 33.58°, 39.37°, 46.35°, and 48.98° displayed by the collected solid indicated the successful conjugation of DBBM with **DNIC-COOH** yielding DNIC-DBBM.

**Reaction of DBBM with complex $[(NO)_2Fe(\mu\text{-}SCH_2CH_2OH)_2Fe(NO)_2]$.** Reaction of DBBM with complex $[(NO)_2Fe(\mu\text{-}SCH_2CH_2OH)_2Fe(NO)_2]$ was attempted following the procedure described above. After reaction of DBBM (0.100 g) with complex $[(NO)_2Fe(\mu\text{-}SCH_2CH_2OH)_2Fe(NO)_2]$ (0.010 g, 0.026 mmol) in THF, absence of the distinctive IR $\nu_{NO}$ absorption peaks displayed by the treated DBBM indicated the failed conjugation of DBBM with complex $[(NO)_2Fe(\mu\text{-}SCH_2CH_2OH)_2Fe(NO)_2]$.

**Preparation of DNIC-TCP and DNIC-COONa-TCP.** To a 15-mL centrifuge tube loaded with TCP (0.100 g) and **DNIC-COOH** (0.007 g, 0.016 mmol), 2 mL of THF was added via stainless cannula under positive $N_{2(g)}$ pressure. This reaction solution was then shaken at ambient temperature for 10 min before being dried under vacuum. Similar to the preparation of DNIC-DBBM, the distinctive IR $\nu$NO stretching frequencies at 1793, 1765, 1730, and 1698 $cm^{-1}$ displayed by the collected solid

indicated the successful preparation of DNIC-TCP. DNIC-COONa-TCP was prepared through reaction of **DNIC-COONa** (0.007 g, 0.016 mmol) and TCP (0.100 g) in a similar manner.

**Release of DNIC from DNIC-DBBM (or DNIC-TCP/DNIC-COONa-TCP) in PBS.** 1 mL of PBS was added to a 2-mL Eppendorf tube loaded with 4 mg of DNIC-DBBM. After the PBS solution of DNIC-DBBM was incubated for 0.5, 10, 20, 30, 40, 50, and 60 min, respectively, at 37°C, the supernatant solution was collected and replaced with 1 mL of fresh PBS. Meanwhile, UV-vis spectrum of the collected supernatant solution, with appropriate dilution, was measured, whereas the absorbance at 362 nm was further adopted to quantify the time-dependent release of **DNIC-COOH**. Based on three independent experiments, the average loading capacity (wt%) of **DNIC-COOH** in DNIC-DBBM was calculated as 6.8±0.3 wt% based on the equation (1) shown below:

$$\text{Loading capacity (wt\%)} = \frac{\text{weight of released DNIC (mg)}}{\text{weight of DNIC - DBBM (mg)}} \times 100\% \quad (1)$$

After the complete release of **DNIC-COOH** from DNIC-DBBM, the residual solid was collected and dried under vacuum. Moreover, solid-state IR spectrum, PXRD patterns, SEM image, elemental mapping, and EDS analysis of the insoluble solid, namely the degraded DNIC-DBBM after complete release of **DNIC-COOH**, were also measured. Time-dependent release of DNIC from DNIC-TCP or DNIC-COONa-TCP in PBS was also investigated in a similar manner.

**Animals, Surgical Procedures, and Experimental Groups.** Male Sprague Dawley rats (about 3 to 4 months of age) weighing from 300 to 400 g were used in this study. The experiment protocols were approved by the Institutional Animal Care and Use Committee (IACUC) of Chang Gung Memorial Hospital (Approval No: 2018120701) and were conducted according to the Principles of Laboratory Animal Care and Guide for the Care and Use of Laboratory Animals published by the National Institutes of

Health. All animals received humane care and were housed in individual cages with controlled temperature, humidity, and 12 h cycles of light and dark, and fed standard chow and tap water *ad libitum*.

After fasting for 8 to 12 hours, gas anesthesia with isoflurane 2.5% to 4.5% was used for induction, followed by 1% to 3% in maintenance after completion of intubation. The animal was placed in a laying position and the surgical area was disinfected with iodophor solution before the local analgesics injection of 2% Lidocaine. After hair shaving and full-thickness flap reflection, a critical-size bone defect, 8 mm in diameter, was created by trephine bur in the rat calvaria. The respective investigated material was grafted in the surgically created calvaria defect accordingly. The flap was closed primarily after the implantation of the planned materials.

After the buildup of rat calvaria bone defects, the rats were further randomly divided into six groups: (1) sham control group, no treatment; (2) TCP group, implantation of 40 mg of TCP; (3) DBBM group, implantation of 40 mg of DBBM; (4) DNIC group, implantation of 2.8 mg of **DNIC-COOH**; (5) DNIC-TCP group, implantation of 40 mg of DNIC-TCP; and (6) DNIC-DBBM group, implantation of 40 mg of DNIC-DBBM. Animals were sacrificed at the $4^{th}$ week (n = 6 for each group) and $12^{th}$ weeks (n = 6 for each group).

**Micro-computed Tomography (micro-CT) Survey.** Live micro-CT (NanoScan® SPECT/CT. Mediso, Hungary) was used to record the calvaria defect with respectively implanted materials immediately after surgery (0 week) under anesthesia in individual rats. Following micro-CT images of each animal were taken at the post-operative fourth week ($4^{th}$ weeks) and the twelfth week ($12^{th}$ week) under anesthesia before sacrifice. No X-ray contrast media was used in this study. The micro-CT images were taken under the following settings: a number of projections 720, X-ray power 50 kVp 980 μA,

exposure time: 170 ms, binning 1:1, voxel size 125*125*125 μm. Visualization, reconstruction, and volume analysis of the data were performed using the PMOD version 4.0 (PMOD Technologies Ltd., Zurich, Switzerland).

The calvaria bone defect was identified at coronal, sagittal, and axial views (Figure S7). The cylindrical volume of interest (VOI), measuring 8 mm in diameter and 875 μm in height, was marked in accordance with the calvaria bone defect. Tissues in the VOI were segmented and analyzed according to the global thresholds of the Hounsfield unit (HU).[3] A HU range of >2700 was utilized to identify the compact bone, whereas the total volume of the compact bone in VOI ($V_t$) was determined to evaluate the bone repair.[4] The data were acquired by the software PMOD version 4.0 (PMOD Technologies Ltd., Zurich, Switzerland). 3D CT images were reconstructed by the software InterView® Fusion (Version 3.03, Mediso Medical Image System, Budapest, Hungary).

**Immunohistochemical (IHC) Analysis.** Animals were sacrificed at post-operative 4$^{th}$ and 12$^{th}$ weeks. The calvaria was removed and initially fixed in 10% phosphate-buffered formalin. Specimens were decalcified with Plank-Rychlo's solution and further fixed with 4% paraformaldehyde. All decalcified samples were paraffin-embedded and then sectioned to the thickness of 3 to 5 μm with a rotary microtome (Leica RM2135, USA). For IHC staining, the tissue sections were deparaffinized and rehydrated prior to incubation with the respective primary antibody, including anti-alpha smooth muscle actin (1:1000, ab7817, Abcam, UK), anti-osteopontin antibody (1:200, ab216402, Abcam, UK), anti-osteocalcin antibody [OCG3] (1:200, ab13420, Abcam, UK), ALPL polyclonal antibody (1:100, E-AB-40142, Elabscience, USA), and anti-vascular endothelial growth factor A (1: 100, ab1316, Abcam, UK) for 1.5 h. After

a triple and 5-min rinse using PBS with Tween™ 20 (PBS-T), sections were then incubated with a Rabbit Anti-Mouse IgG/HRP (horseradish peroxidase) secondary antibody (Dako, CA) for another 45 minutes. Positive immunoreactivity was detected using a diaminobenzidine reagent (DAB. Dako, CA). Photomicrographs were taken with a fluorescence microscope (ZEISS Axio Scope A1, Germany) and the area measurements were performed with the Image-Pro Premier software (Media Cybernetics, Rockville, USA). For IHC staining analysis, the staining of the undegraded bone graft materials was excluded and only regenerated bone tissue was counted. The respective proportions of each biomarker were acquired by dividing the positive staining area by the total area in the surgical bony defect.

**Statistical analysis.** Quantitative data were presented as the mean ± SD and were analyzed with the one-way ANOVA for the intergroup comparisons of cell viability, micro-CT, and IHC analyses in the GraphPad Prism 9.1.1 software (GraphPad Software Inc., San Diego, CA, USA), and a value of $P < 0.05$ was considered statistically significant.

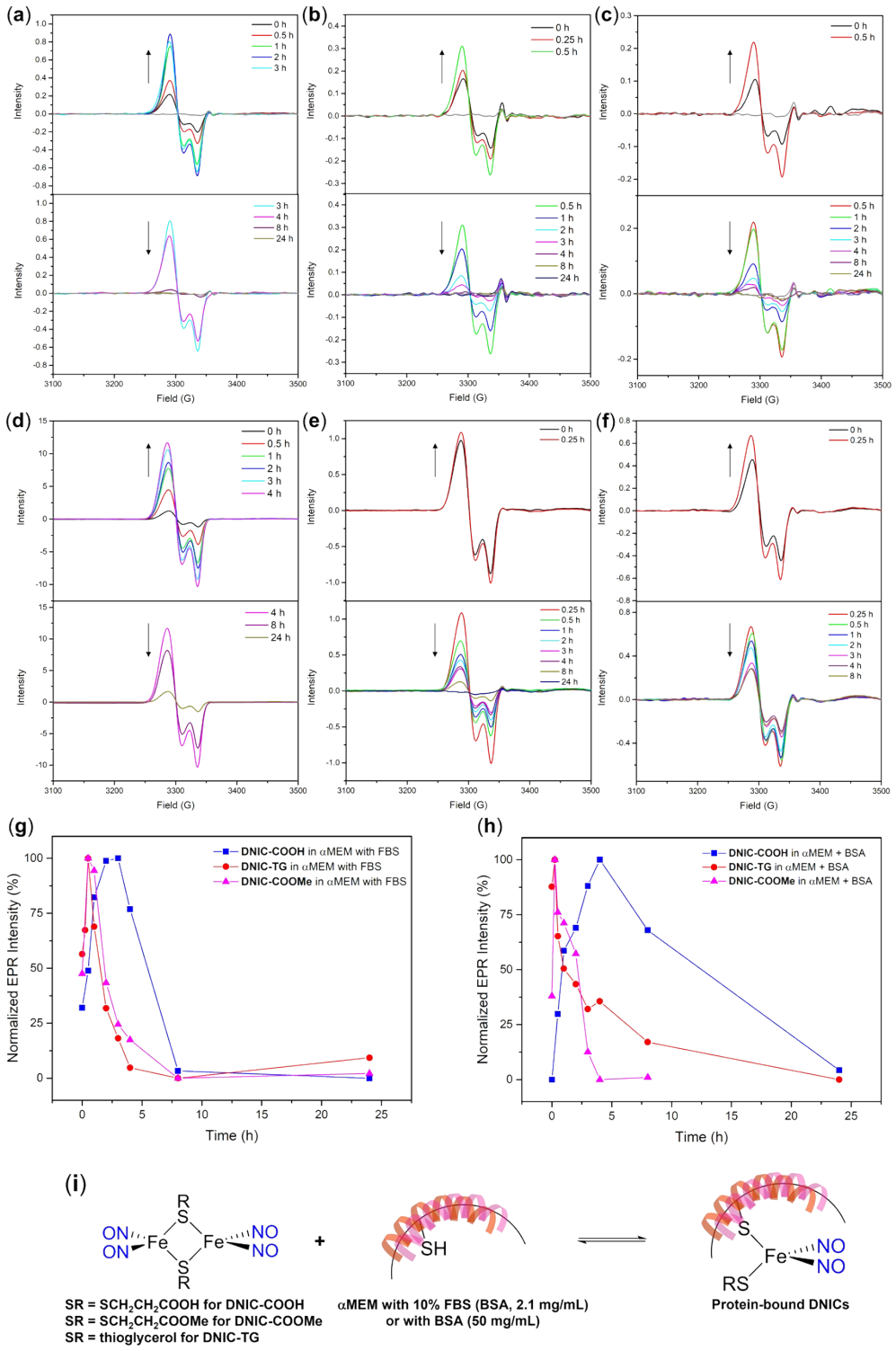


**Figure S1.** Time-dependent change of EPR spectra for (**a**) **DNIC-COOH**, (**b**) **DNIC-TG**, and (**c**) **DNIC-COOMe** in αMEM with 10% FBS. EPR spectra for **DNIC-COOH**, **DNIC-TG**, and **DNIC-COOMe** in αMEM are depicted in gray. Time-dependent change of EPR spectra for (**d**) **DNIC-COOH**, (**e**) **DNIC-TG**, and (**f**) **DNIC-COOMe** in αMEM with the presence of BSA (50 mg/mL). Formation and decay of BSA-bound DNIC derived from the reaction of BSA with **DNIC-COOH** (blue), **DNIC-TG** (red),

and **DNIC-COOMe** (magenta), respectively, in (**g**) αMEM with 10% FBS and (**h**) BSA (50 mg/mL) at 37 °C. (**i**) Schematic illustration for reversible interaction between dinuclear DNICs and BSA leading to the assembly of protein-bound DNICs in αMEM with 10% FBS (BSA, 2.1 mg/mL) or with BSA (50 mg/mL).

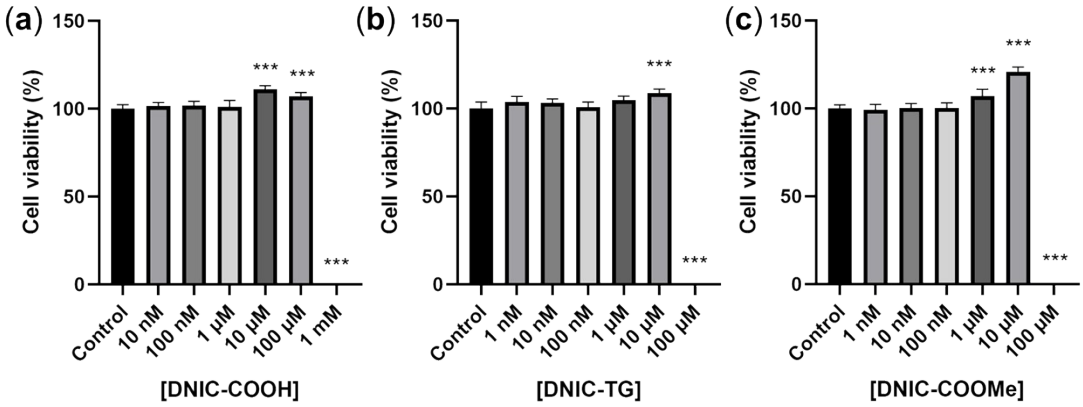


**Figure S2.** Cell viability assay of the MC3T3-E1 osteoblast cells treated with different concentrations of (**a**) **DNIC-COOH**, (**b**) **DNIC-TG**, and (**c**) **DNIC-COOMe** for 24 h. Data represent the mean ± SD (n = 3). $^{*}P < 0.05$ and $^{***}P < 0.001$ compared to the untreated groups.

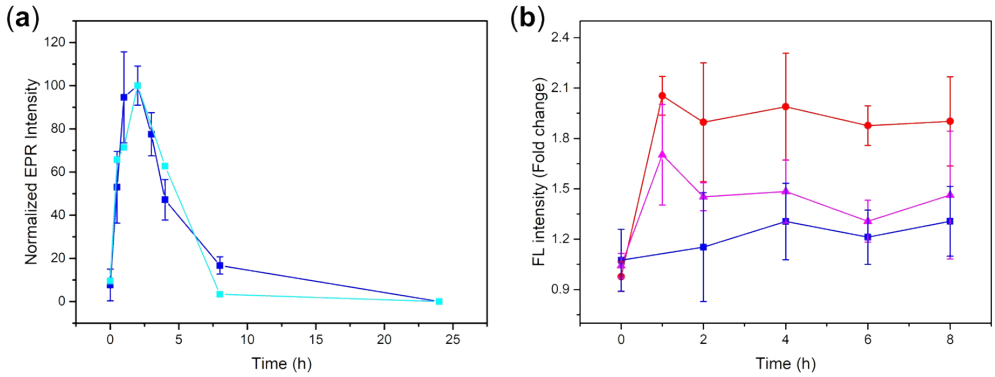


**Figure S3.** (**a**) Formation and decay of intracellular protein-bound DNIC upon treatment of 100 μM (blue) or 10 μM (light blue) of **DNIC-COOH** to osteoblast MC3T3-E1 cells at 37 °C. (**b**) Kinetics for intracellular release of NO after treatment of **DNIC-COOH** (10 μM, blue), **DNIC-TG** (10 μM, red), and **DNIC-COOMe** (10 μM, magenta), respectively, to MC3T3-E1 osteoblast cells at 37 °C, which were pre-treated with DAF-FM (5 μM). The fluorescence intensity was normalized to that of MC3T3-E1 cells treated with only DAF-FM (5 μM). Data represent the mean ± SD (n = 3).

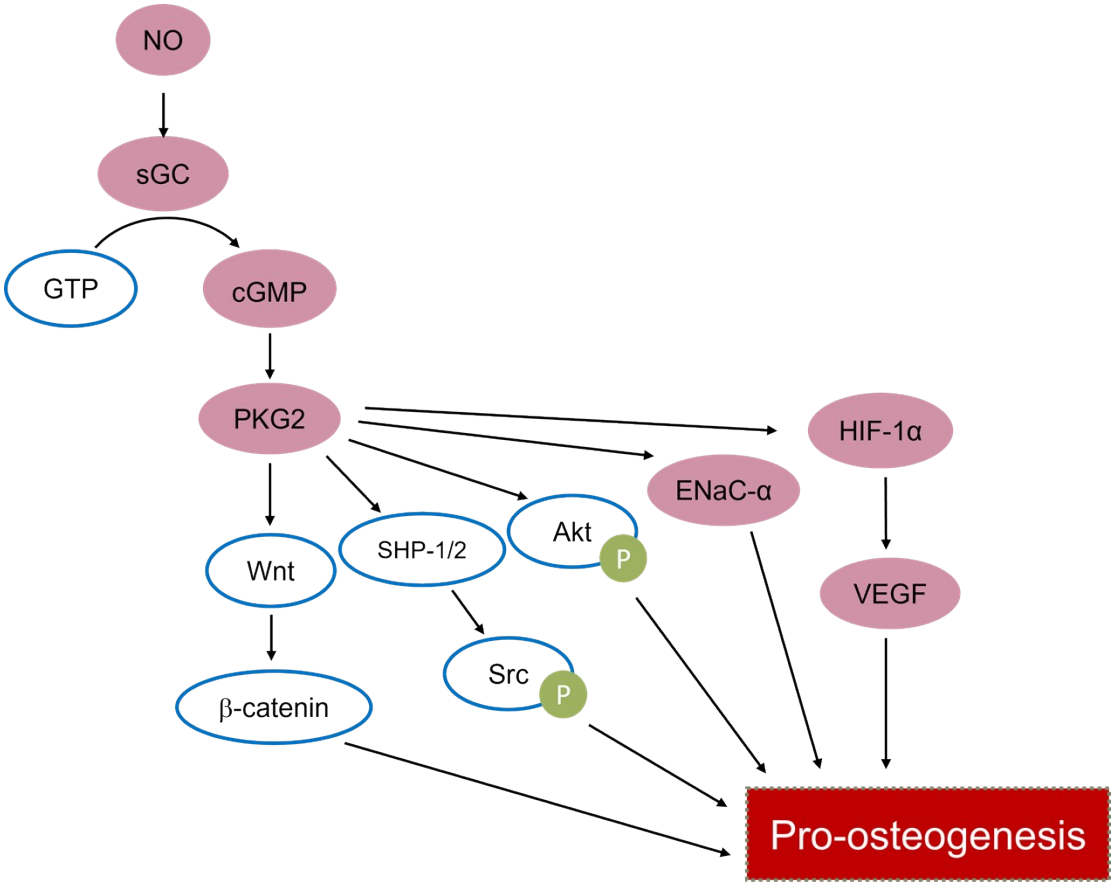


**Figure S4.** Signaling pathways for pro-osteogenesis activity of NO.[5-18]

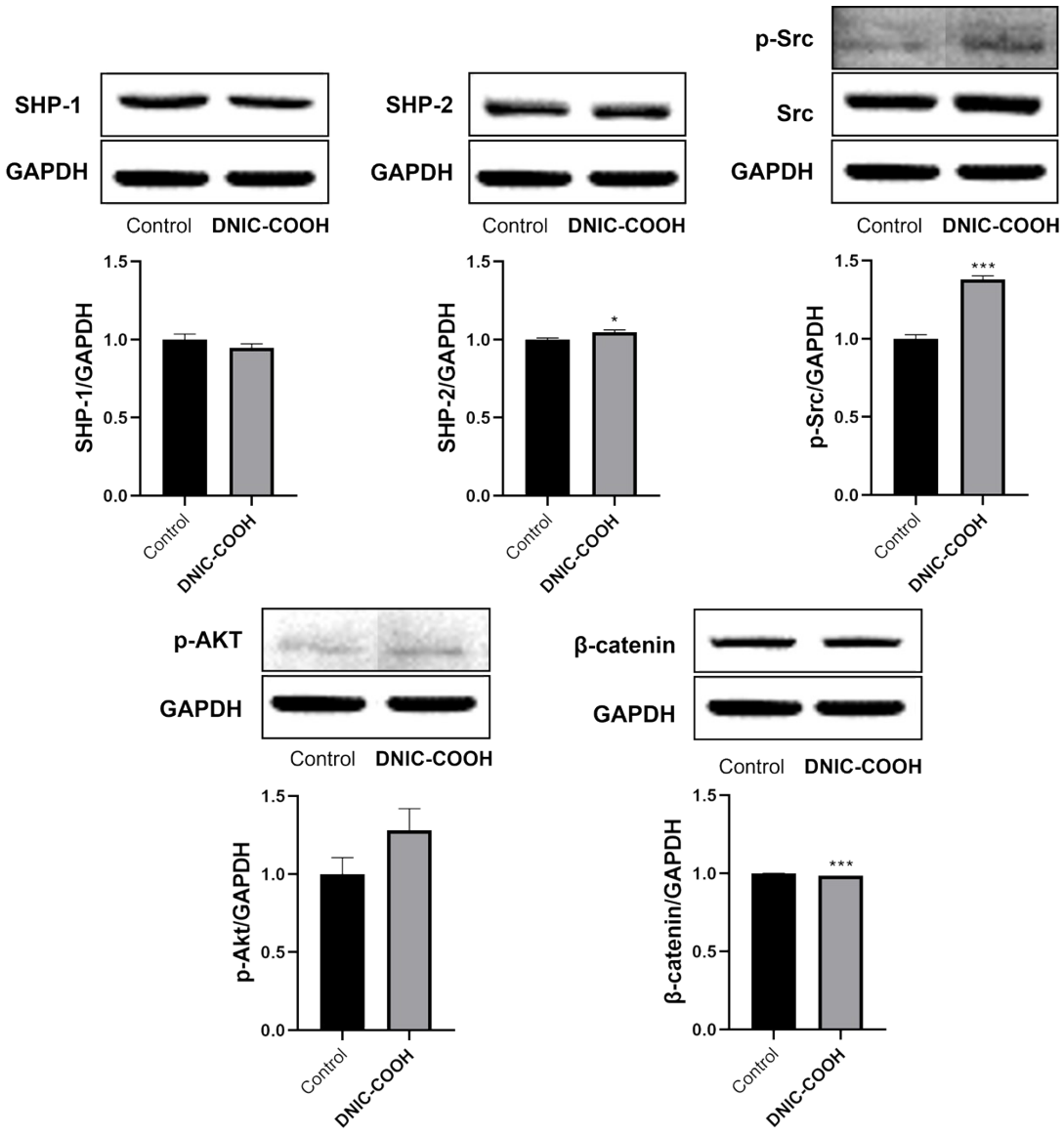


**Figure S5.** Western blot analysis on SHP-1, SHP-2, Src/p-Src, p-Akt, and β-catenin in MC3T3-E1 osteoblast cells after treatment of **DNIC-COOH** (100 μM). The data are the mean values ± SEM (n = 3 for each group).

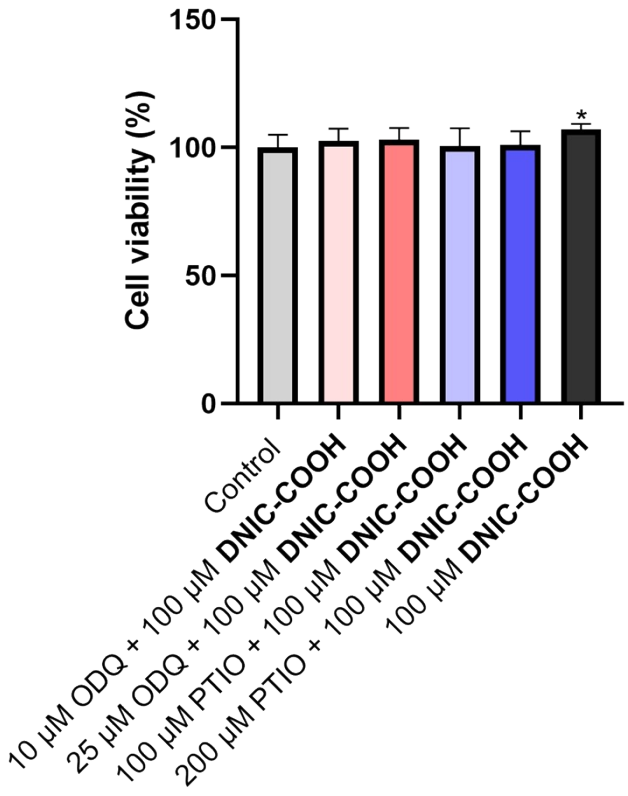


**Figure S6.** Cell viability assay of the MC3T3-E1 osteoblast cells with sequential treatments of ODQ and **DNIC-COOH** or co-treatments of PTIO and **DNIC-COOH** for 24 h. Data represent the mean ± SD (n = 3). $^{*}P < 0.05$ compared to the untreated groups.

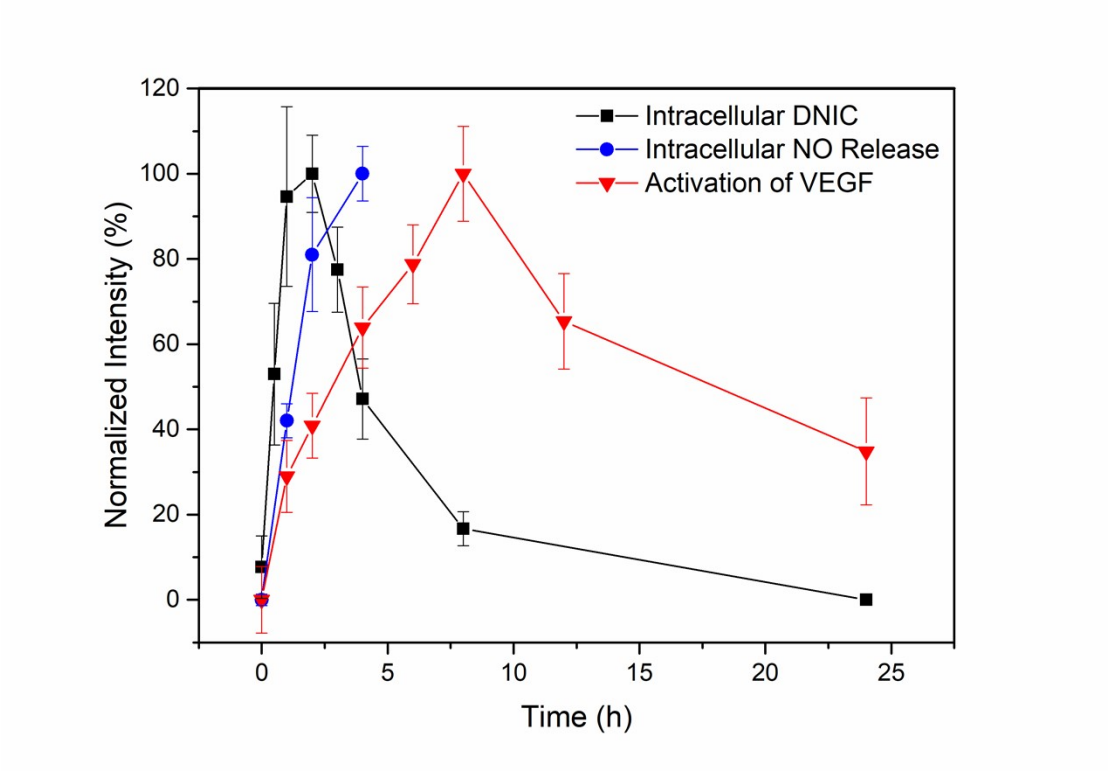


**Figure S7.** Kinetic profiles for cellular uptake of **DNIC-COOH** and intracellular assembly of protein-bound DNICs (black), intracellular release of NO (blue), and activation of VEGF (red) in MC3T3-E1 osteoblast cells after treatment of 100 μM of **DNIC-COOH**.

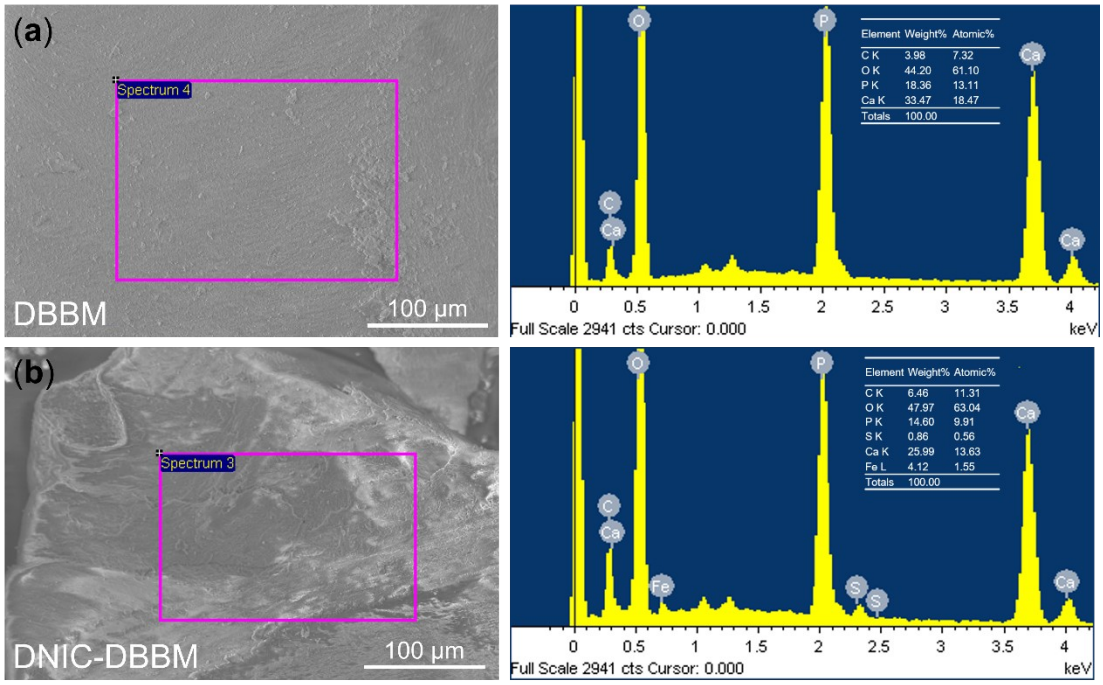


**Figure S8.** SEM images and EDS spectra of (**a**) DBBM and (**b**) DNIC-DBBM.

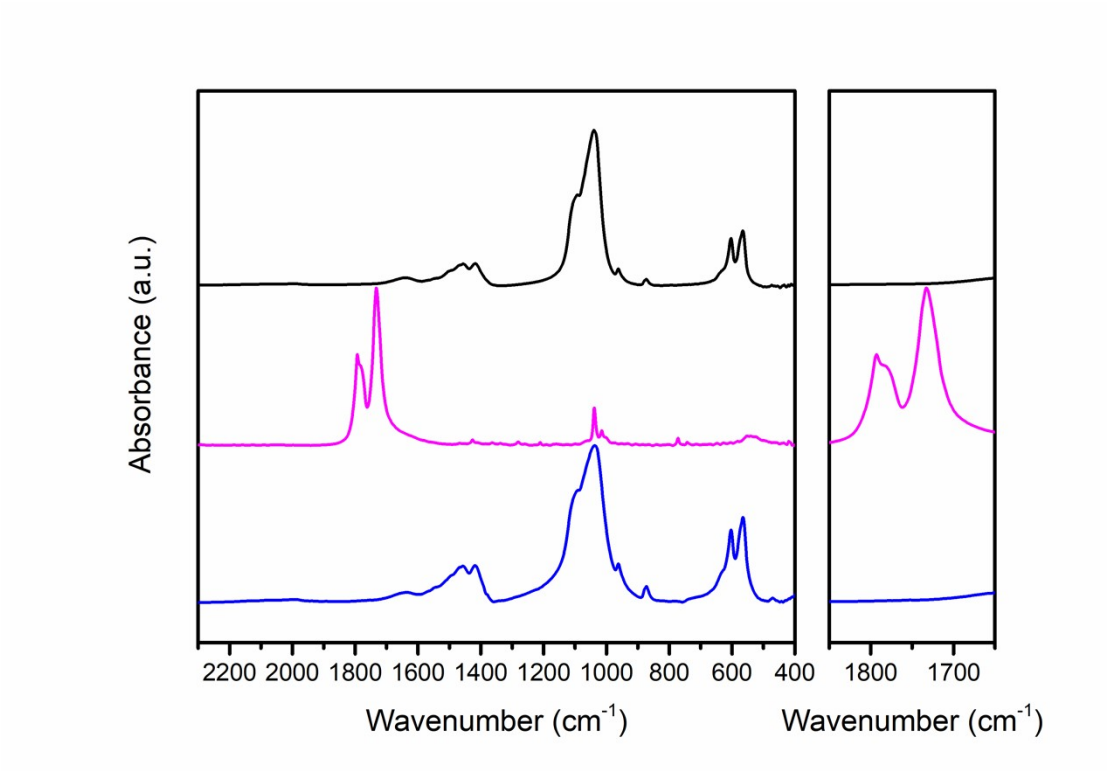


**Figure S9.** Solid-state IR spectra of DBBM before (black) and after its reaction with complex $[Fe_2(\mu\text{-}SCH_2CH_2OH)_2(NO)_4]$ in THF (blue). Solid-state IR spectrum of complex $[Fe_2(\mu\text{-}SCH_2CH_2OH)_2(NO)_4]$ is shown in magenta.

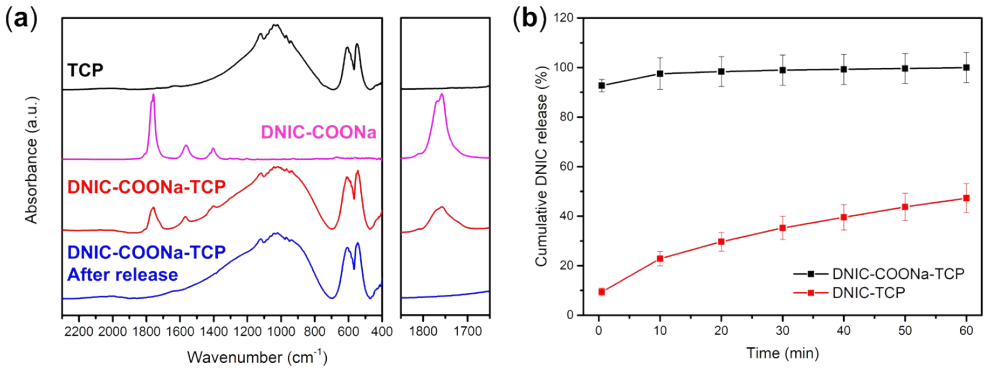


**Figure S10.** (**a**) Solid-state IR spectra for TCP (black) and DNIC-COONa-TCP (red), whereas that of DNIC-COONa-TCP after its incubation in PBS for 60 min is depicted in blue. Solid-state IR spectrum of **DNIC-COONa** is shown in magenta. (**b**) Cumulative release of DNIC from DNIC-COONa-TCP (black) and DNIC-TCP (red) in PBS. Data show the mean ± SD from three independent experiments.

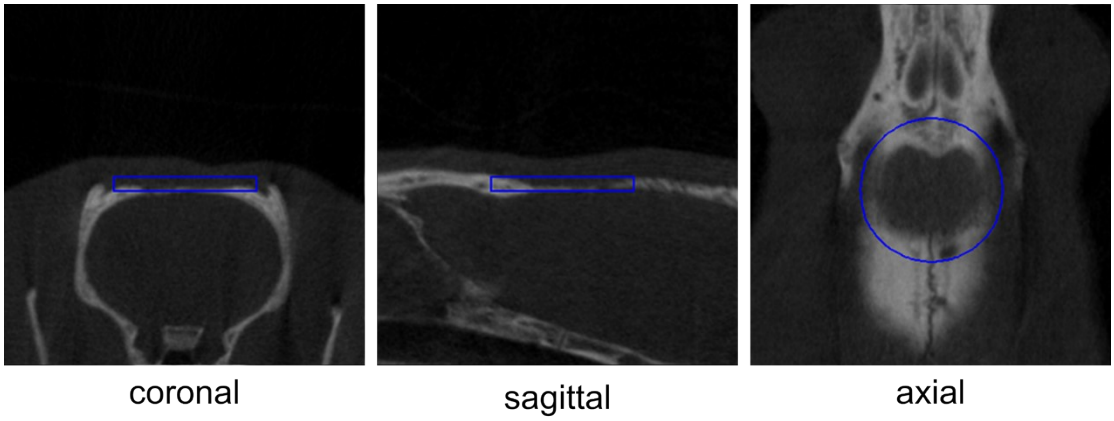


**Figure S11.** Representative micro-CT images in the coronal, sagittal, and axial planes of rats calvaria bone defect. Volume of interest (VOI, 8 mm in diameter and 875 μm in height) is highlighted in blue lines.

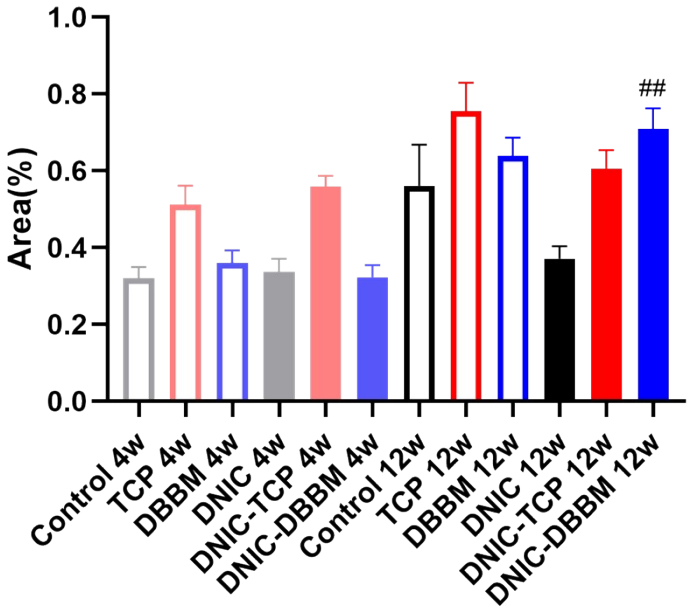


**Figure S12.** IHC analysis on osteocalcin (OCN) of rats with calvaria bone defect under different treatments. The data are the mean values ± SEM (n = 6 for each group). ##: $p<0.01$ for comparison with DNIC group

**Table S1.** Chemical compositions of (simulated) biological fluids, cell culturing media, and aqueous buffer solution.

| Component | Serum | MEM[a] | αMEM[a] | FBS[a] | SGF[b] (USP) | SIF[c] (USP) | Phosphate Buffer |
|---|---|---|---|---|---|---|---|
| pH | ~7.4 | ~7.4 | ~7.4 | 6.5-8.5 | 1.2 | 6.8 | - |
| $Cl^-$ (mM) | 100 | 127.6 | 127.0 | 99 | ~118 | - | - |
| $HCO_3^-/H_2CO_3$ (mM) | 24 | 26.2 | 26.2 | - | - | - | - |
| $HPO_4^{2-}/H_2PO_4^-$(mM) | 1.2 | 1.0 | 1.0 | 3.07 | - | 50 | 50 |
| $SO_4^{2-}$ (mM) | 0.33 | 0.8 | 0.8 | - | - | - | - |
| $Na^+$ (mM) | 140 | 144.8 | 145.9 | 136 | 34.2 | 22.4 | - |
| $K^+$ (mM) | 4.5 | 5.3 | 5.3 | >10 | - | 50 | 75 |
| $Ca^{2+}$ (mM) | 1.4 | 1.8 | 1.8 | 3.4 | - | - | - |
| $Mg^{2+}$ (mM) | 0.52 | 0.8 | 0.8 | - | - | - | - |
| Glucose (mM) | 5.0 | 5.6 | 5.6 | 5.5 | - | - | - |
| Protein (total, mg/mL) | 70 | - | - | 30-45 | 3.2 | 10 | - |
| Albumin (mM) | 0.63 | - | - | <0.68 | - | - | - |
| Urea (mM) | - | - | - | 2.33 | - | - | - |
| Iron (mM) | - | - | - | 0.005 | - | - | - |
| Amino acids (μM) | 10-400 | 3428 | 8535 | - | - | - | - |
| L-cysteine (μM) | - | - | 568.2 | - | - | - | - |
| Ascorbic acid (μM) | - | - | 284.1 | - | - | - | - |

[a]Chemical compositions of MEM and αMEM, and selected chemical compositions of FBS were obtained from the product data sheet. [b]simulated gastric fluid. [c]simulated intestinal fluid.

**Reference**


1. S.-L. Cho, C.-J. Liao and T.-T. Lu, *J. Biol. Inorg. Chem.*, 2019, **24**, 495-515.
2. C.-W. Chung, B.-W. Liao, S.-W. Huang, S.-J. Chiou, C.-H. Chang, S.-J. Lin, B.-H. Chen, W.-L. Liu, S.-H. Hu, Y.-C. Chuang, C.-H. Lin, I.-J. Hsu, C.-M. Cheng, C.-C. Huang and T.-T. Lu, *ACS Appl. Mater. Interfaces*, 2022, **14**, 6343-6357.
3. K. L. Beaucage, S. I. Pollmann, S. M. Sims, S. J. Dixon and D. W. Holdsworth, *Bone Rep.*, 2016, **5**, 70-80.
4. L. Z. Di, V. Couture, E. Leblanc, Y. Alinejad, J. F. Beaudoin, R. Lecomte, F. Berthod, N. Faucheux, F. Balg and G. Grenier, *Adv. Orthop.*, 2014, **2014**, 791539.
5. J. W. Denninger and M. A. Marletta, *Biochim. Biophys. Acta*, 1999, **1411**, 334-350.
6. J. Chen, H. Zhang, X. Zhang, G. Yang, L. Lu, X. Lu, C. Wan, K. Ijiri, H. Ji and Q. Li, *Mol. Biol. Rep.*, 2014, **41**, 2161-2169.
7. H. Rangaswami, R. Schwappacher, N. Marathe, S. Zhuang, D. E. Casteel, B. Haas, Y. Chen, A. Pfeifer, H. Kato, S. Shattil, G. R. Boss and R. B. Pilz, *Sci. Signal.*, 2010, **3**, ra91.
8. N. Marathe, H. Rangaswami, S. Zhuang, G. R. Boss and R. B. Pilz, *J. Biol. Chem.*, 2012, **287**, 978-988.
9. Y. K. Zhai, X. Y. Guo, B. F. Ge, P. Zhen, X. N. Ma, J. Zhou, H. P. Ma, C. J. Xian and K. M. Chen, *Bone*, 2014, **66**, 189-198.
10. H. Kalyanaraman, N. Schall and R. B. Pilz, *Nitric Oxide*, 2018, **76**, 62-70.
11. H. Kalyanaraman, G. Ramdani, J. Joshua, N. Schall, G. R. Boss, E. Cory, R. L. Sah, D. E. Casteel and R. B. Pilz, *J. Bone Miner. Res.*, 2017, **32**, 46-59.
12. G. Ramdani, N. Schall, H. Kalyanaraman, N. Wahwah, S. Moheize, J. J. Lee, R. L. Sah, A. Pfeifer, D. E. Casteel and R. B. Pilz, *J. Endocrinol.*, 2018, **238**, 203-219.
13. T. Yan, Y. Xie, H. He, W. Fan and F. Huang, *Int. J. Mol. Med.*, 2021, **48**.
14. A. P. Kusumbe, S. K. Ramasamy and R. H. Adams, *Nature*, 2014, **507**, 323-+.
15. S. Pal, M. Rashid, S. K. Singh, K. Porwal, P. Singh, R. Mohamed, J. R. Gayen, M. Wahajuddin and N. Chattopadhyay, *Bone*, 2020, **135**, 115305.
16. W. Gotz, C. Reichert, L. Canullo, A. Jager and F. Heinemann, *Ann. Anat.*, 2012, **194**, 171-173.
17. Y. Wang, C. Wan, L. Deng, X. Liu, X. Cao, S. R. Gilbert, M. L. Bouxsein, M. C. Faugere, R. E. Guldberg, L. C. Gerstenfeld, V. H. Haase, R. S. Johnson, E. Schipani and T. L. Clemens, *J. Clin. Invest.*, 2007, **117**, 1616-1626.
18. F. S. Wang, Y. R. Kuo, C. J. Wang, K. D. Yang, P. R. Chang, Y. T. Huang, H. C. Huang, Y. C. Sun, Y. J. Yang and Y. J. Chen, *Bone*, 2004, **35**, 114-123.